

Thermal diffusion and chemical kinetics in laminar biomaterial due to heating by a free-electron laser

M. Shane Hutson, Susanne A. Hauger, and Glenn Edwards*

Free Electron Laser Laboratory and Department of Physics, Duke University, Box 90319, Durham, North Carolina 27708

(Received 9 October 2001; revised manuscript received 7 March 2002; published 17 June 2002)

We have theoretically investigated the role of thermal diffusion and chemical kinetics as a possible dynamic explanation for the preferential ablative properties of infrared radiation from a free-electron laser (FEL). The model is based on a laminar system composed of alternating layers of protein and saline. We have compared exposure to 3 μm where water is the main absorber and 6.45 μm where both water and protein absorb. The picosecond pulses of the superpulse are treated as a train of impulses. We find that the heating rates are sufficient to superheat the outer saline layers on the nanosecond time scale, leading to explosive vaporization. We also find that competition between the layer-specific heating rates and thermal diffusion results in a wavelength-dependent separation in layer temperatures. We consider the onset of both chemical bond breaking and the helix-coil transition of protein prior to vaporization in terms of the thermal, chemical, and structural properties of the system as well as laser wavelength and pulse structure. There is no evidence for thermal bond breaking on these time scales. At 6.45 μm , but not 3 μm , there is evidence for a significant helix-coil transition. While the native protein is ductile, the denatured protein exhibits brittle fracture. This model provides a dynamic mechanism to account for the preferential ablative properties observed with FEL radiation tuned near 6.45 μm .

DOI: 10.1103/PhysRevE.65.061906

PACS number(s): 87.50.Hj; 44.05.+e; 82.39.-k

I. INTRODUCTION

Experiments demonstrate that the free-electron laser (FEL) is a particularly effective tool for etching soft biomaterials with remarkably little damage surrounding the site when tuned to wavelengths near 6.45 μm [1]. Based on these observations, human neurosurgical [2] and ophthalmic [3] procedures were developed and have been performed successfully. As for the underlying physical mechanism, these results cannot be accounted for with models solely based on average penetration depth. A thermodynamic model has been proposed to account for the wavelength dependence suggesting that the optical, thermal, and mechanical properties of protein as distinct from saline are important [1]. However, the dynamics and how they relate to the superpulse structure of the Mark-III have not been well understood.

Here we present a dynamic theory to account for the wavelength and pulse-structure dependence in terms of thermal diffusion and chemical kinetics in a laminar system that is highly representative of cornea as exposed to FEL radiation. We find that the competition between the layer-specific heating rates and thermal diffusion results in a wavelength-dependent separation in layer temperatures that increases on the nanosecond time scale. As a consequence, significantly more protein denaturation accumulates at 6.45 μm than at 3 μm . Native protein is ductile, whereas denatured protein is brittle. We attribute the preferential ablative properties of the FEL, tuned to wavelengths near 6.45 μm , to the brittle nature of denatured collagen.

II. THEORETICAL MODEL

We have chosen to model cornea for two reasons. First, there is extensive experimental data to support the model [4–10]. Second, the regularity of its structure allows a relatively detailed theoretical treatment. Cornea is predominantly composed of highly ordered, alternating sheets of the protein collagen and water, each about 30 nm thick. Collagen molecules are assembled in cylindrical bundles, each 22–32 nm in diameter, which are aligned and close packed in the protein sheets.

The FEL produces a superpulse, i.e., a 2–6 μs burst of picosecond pulses at a repetition rate of 2.85 GHz [11]. Superpulses are typically repeated at 10–30 Hz. FEL experiments demonstrate that material removal begins within the superpulse on the 100-ns time scale [12]. Since thermal diffusion over a distance of 30 nm in an aqueous environment occurs with a relaxation time of about 850 ps [13], the picosecond pulses may be idealized as impulses to a good approximation. On the other hand, the 350-ps pulse separation was considered explicitly.

Thermal diffusion is typically described with Fourier's equation, where laser heating of the medium is accounted for by an additional source term Q , to yield the heat balance equation,

$$\rho c_p \frac{\partial T}{\partial t} = \kappa \nabla^2 T + Q, \quad (1)$$

where ρ is the density, c_p is the specific heat at constant pressure, T is the temperature, and κ is the thermal conductivity [14]. We apply the heat balance equation to a laminar system representative of cornea. The specific geometry is a half space of air ($z < 0$) overlying 500 alternating 30-nm

*Corresponding author. FAX: (919)-660-2671. Email address: edwards@fel.duke.edu

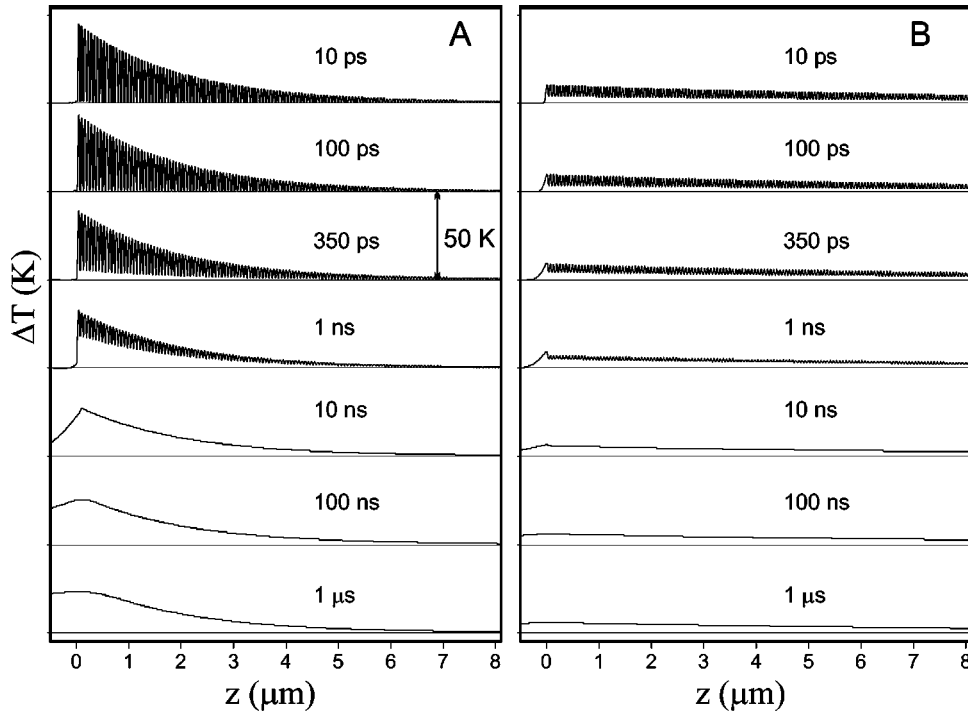


FIG. 1. Thermal response to a single impulse at (A) 3 and (B) 6.45 μm . The range for each trace is 50 K, as shown for the case of 3 μm and 350 ps. The absorption depth for protein is 100 μm (8 μm) and for saline is 1 μm (12 μm) at wavelengths of 3 μm (6.45 μm), respectively [1]. The refractive index is 1.00 for air and is uniformly 1.35 for cornea. The density is 1540, 1000, and 1.29 kg m^{-3} , the specific heat is 1560, 4184, and 1005 $\text{J kg}^{-1} \text{K}^{-1}$, and the thermal conductivity is 0.195, 0.602, and 0.0292 $\text{W m}^{-1} \text{K}^{-1}$, for protein, saline, and air, respectively [5].

layers of protein and saline ($0 < z < 15 \mu\text{m}$) with a semi-infinite saline substrate ($z > 15 \mu\text{m}$). The protein has the optical and thermal properties of collagen, and both air and saline are characterized by distinctive optical and thermal properties [1,5]. Differential absorption as well as reflection and interference are taken into account to determine the spatial pattern of heat deposition in each layer [15]. Scattering of midinfrared radiation is a small effect and is not included. Laser irradiation is normal to the layer surfaces with a Gaussian profile ($1/e^2$ radius of 50 μm), i.e., the axisymmetric system reduces the analysis to two dimensions. While the radial thermal relaxation time for a 50- μm spot size is milliseconds [13], our interest is for times shorter than several hundred nanoseconds. Thus, a one-dimensional calculation on the z axis is a good approximation.

The model calculations were performed with local, temporally truncated, axisymmetric Green's functions in Hankel-Fourier space as a modified version [16] of the multilayer thermal diffusion model [17]. To reduce the calculation to one dimension, the conjugate radial variable in Hankel space was set to zero. Thermal responses in Fourier space were calculated with an axial spacing of 6 nm, multiplied by the Fourier transform of the FEL pulse structure, and fast Fourier transformed to yield the temperature rise $\Delta T(z, t)$. The use of a fast Fourier transform required that the temperatures be calculated on an evenly spaced frequency (and thus temporal) lattice. For reasonable calculation times we implemented 2048 lattice points with the temporal truncation of the Greens's functions limiting useful temperature information to the first 512 lattice points. Sets of calculations were run for varying temporal lattice spacings (1 ps, 10 ps, 70 ps, 350 ps, 7 ns, 700 ns or 3.5 μs) depending on the time regime under consideration. Programs to calculate temperature distributions were written in Array Basic and executed with the GRAMS/32 interpreter.

For completeness, we have considered two complications. It has been pointed out that the use of Fourier's equation fails to account for the finite speed of thermal wave propagation, which is accounted for by the hyperbolic heat conduction equation [18]. Our comparison of the two approaches revealed small deviations limited to the first few picoseconds following an impulse. In addition, rapid heating by a picosecond FEL pulse results in transient pressure pulses, tens of MPa in magnitude, that decay within several picoseconds with a small volume expansion and an inconsequential amount of work.

III. RESULTS AND DISCUSSION

A. Laser heating and thermal diffusion

The FEL wavelengths of interest are 3 μm , where water absorbs strongly, and 6.45 μm , where both water and protein absorb [1]. One μJ per impulse is delivered to a Gaussian spot of 50 μm (e^{-2} radius) and the temperature is tracked on the symmetry axis. Figure 1 summarizes the thermal response to a single impulse. Distinctive patterns in temperature are evident from 10 ps through 1 ns due to the differences in absorption for protein and water in this laminar system. Interlayer diffusion and an indication of a surface enhancement are evident on the nanosecond time scale. By 10 ns the temperature profiles are independent of laminar structure. Exponential decay in z due to Beer's law is evident at all times.

It is instructive to introduce some physical concepts to interpret this relatively simple case before proceeding to a consideration of a train of impulses. As shown in Fig. 1, remnants of the layer-specific absorption patterns remain until several nanoseconds after the laser pulse. At 3 μm , the saline layers are relative heat sources and the protein layers are relative heat sinks during that period. In contrast, at

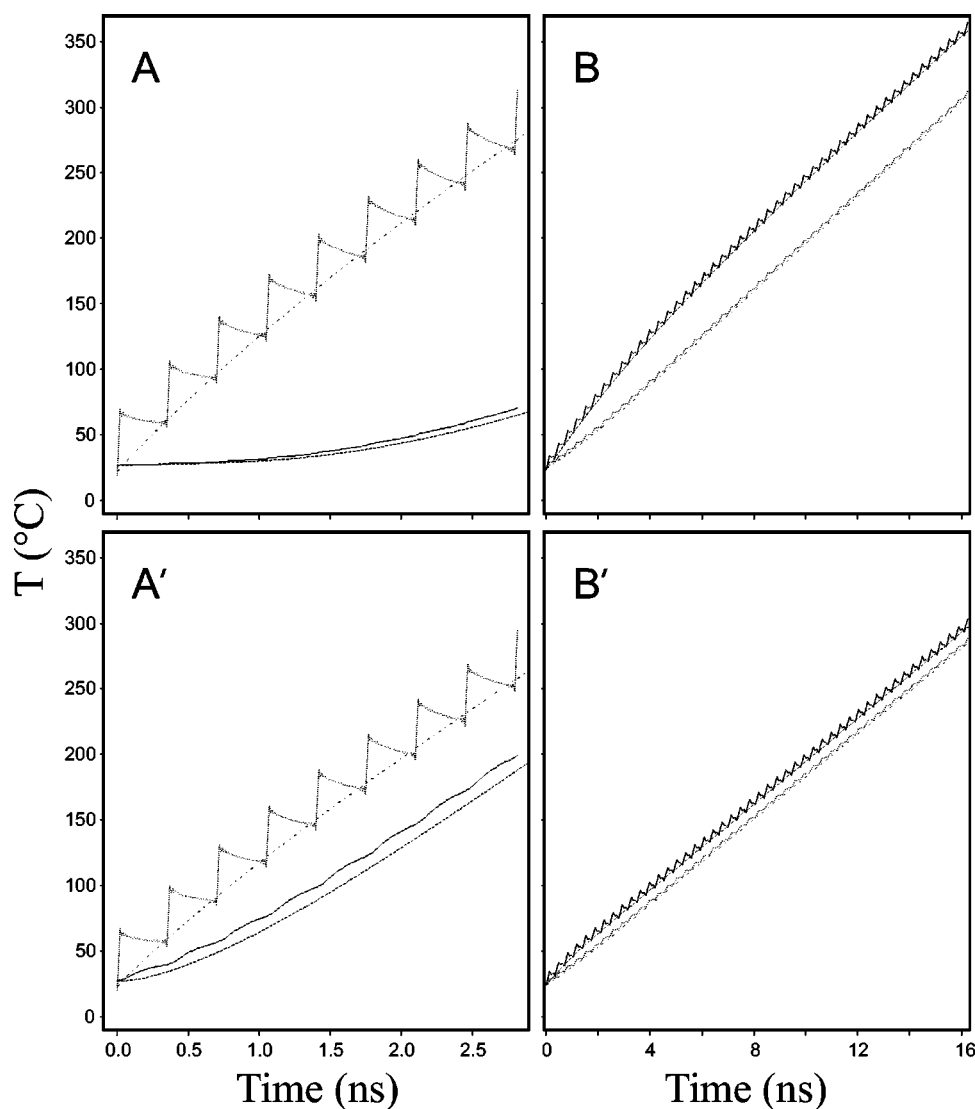


FIG. 2. Thermal response to a train of impulses. Surface layers exposed to (A) 3 and (B) 6.45 μm . Layers 200 nm below the surface exposed to (A') 3 and (B') 6.45 μm . In addition, the FEL superpulse structure, protein (solid) and water (dotted), is compared to a 16.2 ns pulse with the same average energy, protein (dashed) and water (dot dash). The initial temperature was 25 °C.

6.45 μm the protein layers are heat sources relative to the saline layers. Although the air temperature near $z=0$ rises significantly on the nanosecond time scale, this temperature rise results from heat diffusion of only a small fraction of the thermal energy content in the surface protein layer. Due to the much lower density of air, as represented by the respective thermal conductivities, air is not effective as a heat sink. The ratio of $\kappa_{\text{saline}}:\kappa_{\text{protein}}:\kappa_{\text{air}}$ is 21:7:1. Figure 1 indicates that thermal relaxation is incomplete at 350 ps, i.e., when the next pulse arrives in a macropulse.

Figure 2 summarizes the thermal response to a train of such impulses separated by 350 ps, demonstrating a relatively shallow “staircase” or “saw tooth” on a rising background temperature. Competition between the layer-specific rates of energy absorption, i.e., direct laser heating, and the rate of thermal diffusion results in wavelength-dependent temperature differences between adjacent saline and protein layers on the nanosecond time scale. At 3 μm , the laser energy is predominantly absorbed by the saline layers. The rate of direct laser heating outpaces the rate of diffusion losses in the saline layers and consequently the temperatures of the protein layers increasingly lag behind (frames A and A'). At

6.45 μm , significant laser energy is absorbed by both the protein layers, and to a lesser extent, the saline layers. The rate of direct laser heating again outpaces thermal diffusion resulting in a temperature enhancement of the protein layers compared to the adjacent saline layers (frames B and B').

The temperature difference in a neighboring pair of protein and saline layers is exaggerated at the surface (frames A and B) when compared to 200 nm into the material (frames A' and B'). For each wavelength, the temperature of the outermost saline layer is comparable to the subsurface saline layer, which we define as that layer 200 nm below the surface. However, the temperatures of the surface and subsurface protein layers differ significantly. At 3 μm (frames A and A'), the temperature of the surface protein layer lags behind the subsurface protein layer. The temperature of the surface protein layer (frame A), which has only one neighboring heat source, rises more slowly than the subsurface protein layer (frame A') that is sandwiched between two heat sources. This situation is reversed at 6.45 μm (frames B and B'), where the temperature of the surface protein layer exceeds the subsurface protein layer. The temperature of the surface protein layer (frame B), which has only one neigh-

boring heat sink, rises more quickly than the subsurface protein layer (frame B') that is sandwiched between two heat sinks.

Calculations (not shown) in which the surface layer is saline instead of protein show comparable effects. At $3\ \mu\text{m}$, the temperature of the surface saline layer greatly exceeds the underlying saline layers because the surface layer is adjacent to only one protein heat sink. At $6.45\ \mu\text{m}$, the temperature of the surface saline layer lags behind the underlying saline layers because the surface layer is adjacent to only one protein heat source. Thus, the enhancement in the surface temperature differences is due to two features. First, it is a property of laminar materials where the layers have distinct absorption coefficients for the incident radiation. Second, the ambient air layer must be a relatively poor heat sink, i.e., the thermal conductivities of each laminar material must exceed that of air.

A comparison of Figs. 1 and 2 indicates that for these exposure conditions a single impulse will not lead to vaporization. In contrast, a train of impulses with a repetition rate of 2.85 GHz does rapidly heat the saline layers to temperatures well in excess of $100\ ^\circ\text{C}$. Saline is superheated when the volumetric rate of energy deposition q' exceeds the rate at which energy is consumed through the growth of preexisting vapor phase nuclei [19]. This criterion can be written as

$$q' > \rho h_l \Omega V'(t), \quad (2)$$

where ρ is the density of saline, h_l is the latent heat of vaporization, $V'(t)$ is the rate of bubble growth, and Ω is the density of preexisting vapor phase nuclei. For $\Omega = 10^{15}\ \text{m}^{-3}$, the bubbles grow into a continuous vapor phase in 100 ns [20]. Using this estimate of Ω , the exposure conditions at 3 and $6.45\ \mu\text{m}$ satisfy the criterion for superheating by five and three orders of magnitude, respectively. At atmospheric pressure, the spinodal limit for superheated water is theoretically estimated to be $305\ ^\circ\text{C}$ and the highest superheating temperature observed for an aqueous salt solution is $302\ ^\circ\text{C}$ [19]. Thus as shown in Fig. 2, the temperature of the saline layers increases until the onset of homogeneous nucleation of the vapor phase near the spinodal limit, i.e., explosive vaporization.

B. Chemical kinetics

Thermal diffusion in this laminar system needs to be considered in light of several characteristic temperatures as shown in Fig. 3. First, we assume $302\ ^\circ\text{C}$ is the superheat limit for saline. The temperature profiles shown in Fig. 3 correspond to the time at which the hottest saline layer first exceeds this limit. Second, collagen denaturation via the helix-coil transition is broad, with a peak temperature of $65\ ^\circ\text{C}$ [6]. Third, thermogravimetric measurements demonstrate a broad feature with a slow-heating ($3\ ^\circ\text{C}/\text{min}$) peak decomposition temperature of $307\ ^\circ\text{C}$ [7]. This thermal decomposition was found to be a second-order reaction, attributed to breaking of the amide bond. In the following, we will consider the consequences of heating to these critical temperatures on the 10-ns time scale.

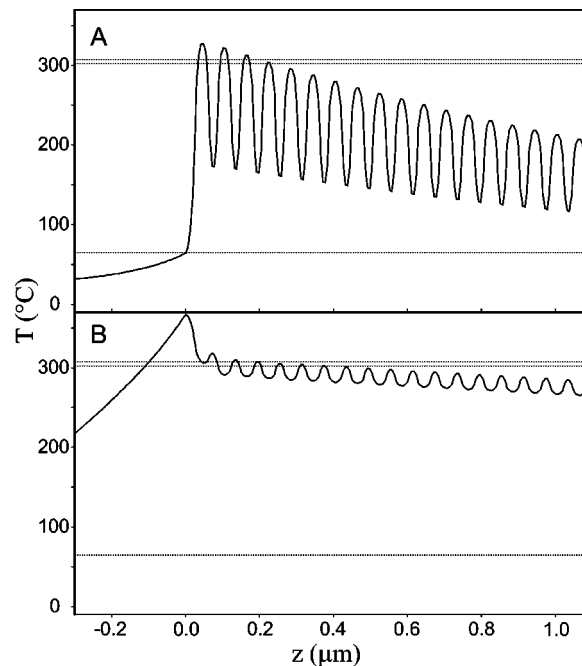


FIG. 3. Thermal response to a train of impulses at (A) 3 and (B) $6.45\ \mu\text{m}$. The initial temperature was $25\ ^\circ\text{C}$. The horizontal lines mark three characteristic temperatures: $65\ ^\circ\text{C}$, $302\ ^\circ\text{C}$, and $307\ ^\circ\text{C}$ (see text).

The kinetics of thermal decomposition can be treated with the Arrhenius model for a second-order reaction,

$$\frac{1}{C} \frac{dC}{dt} = A_2 C e^{-E/RT(t)}, \quad (3)$$

where A_2 is the Arrhenius prefactor, R is the gas constant, E ($82\ \text{kJ}/\text{mol}$) is the activation energy [7], and C ($3.14\ \text{mol}\ \text{L}^{-1}$) is the residue concentration for collagen [8]. We were unable to find a literature value for the prefactor; however, analysis of the thermogravimetric data [7] does yield a good approximation. More specifically, we observed that the concentration of material can be reasonably approximated as inversely proportional to temperature for the decomposition process centered at $307\ ^\circ\text{C}$, yielding a prefactor of $3.0 \times 10^4\ \text{L}\ \text{mol}^{-1}\ \text{s}^{-1}$. This value is consistent with a peak decomposition temperature of $307\ ^\circ\text{C}$ at a heating rate of $3\ ^\circ\text{C}$ per minute. However, the Arrhenius model indicates that essentially no thermal decomposition occurs on the 100-ns time scale for the temperatures indicated in Fig. 3.

Since hydrolysis of the amide bond is an exothermic process [9], we also investigated the possibility of spontaneous thermal explosion [21]. The essential concept underlying thermal explosion is a competition between two processes. The exponential temperature dependence of the exothermic reaction rate, now the heat source under consideration, competes with the linear temperature dependence of heat diffusion, the mechanism for heat loss. If the source overwhelms the loss mechanism, the chemical reaction self-accelerates, rendering the system thermally unstable. In mathematical terms, the resulting transcendental equation does not exhibit a solution for all parameters. The absence of a solution is

taken to be the onset of critical phenomena, in this case acceleration of protein decomposition. The critical parameter δ is geometry dependent, with a value of 0.84 for a disc. The system is thermally stable for δ less than 0.84 and unstable otherwise, where

$$\delta = \frac{QE r^2 A_2 C^2}{\kappa R T^2} e^{-E/RT}. \quad (4)$$

$Q(4.31 \times 10^{-20} \text{ J})$ is the heat release due to the exothermic reaction [9] and r (15 nm) is the characteristic length, i.e., the half-layer thickness. This analysis indicates that for the temperatures summarized in Fig. 3 this system fails to satisfy the criterion for spontaneous thermal explosion by 12 orders of magnitude. This is due in part to the relatively small value for A_2 , which was determined by our reanalysis of the thermogravimetric data [7] as described above.

Having ruled out photothermal bond breaking on the 10-ns time scale, we turn our attention to collagen denaturation. Measurements of the endothermic denaturation of corneal collagen have been accounted for in an approximate fashion with first-order kinetics,

$$\frac{1}{C} \frac{dC}{dt} = \frac{RT(t)}{hN_a} e^{(1+\Delta S^*/R)} e^{-E_a/RT(t)}, \quad (5)$$

where E_a (106 kJ mol^{-1}) is the activation energy and ΔS^* ($39 \text{ J mol}^{-1} \text{ K}^{-1}$) is the activation entropy [5]. Figure 4 plots the fractional collagen denaturation calculated by integration of Eq. (5) up to the time of explosive vaporization. Heating due to $6.45 \mu\text{m}$ radiation results in approximately 1% denaturation in the outer protein layer at the onset of explosive vaporization at 16.2 ns. The amount of denaturation due to $3 \mu\text{m}$ radiation, at the onset of explosive vaporization at 2.8 ns, is a factor of 5000 less. This difference is due to the exponential dependence on inverse temperature. While this analytical treatment is applicable until the onset of explosive vaporization, we can comment on later times. The fractional denaturation will continue to increase up to the onset of material removal, which has been observed on the 100-ns time scale [12]. In addition, during explosive vaporization the energy stored in the superheated liquid is rapidly converted to latent heat, vaporizing $\sim 40\%$ of the saline [19]. The temperature of the saline layer falls towards 100°C , where the temperature is a function of pressure. Furthermore, during vapor expansion the pressure in the saline layers and the stress in the protein layers increase until the outer protein layer(s) mechanically fail. Thermomechanical measurements indicate that collagen is ductile in the laminar regions of cornea with an ultimate tensile strength of approximately 12 MPa, but when thermally denatured this protein exhibits brittle fracture at ultimate tensile strengths around 1 MPa [10]. At $3 \mu\text{m}$ the ductile collagen strains when stressed by the expanding vapor and consequently stores stress energy. Stress increases and propagates until tensile failure, when the stress energy is released and contributes to collateral damage. In contrast, at $6.45 \mu\text{m}$ the brittle denatured collagen fractures when marginally stressed and consequently has a tendency for less collateral damage.

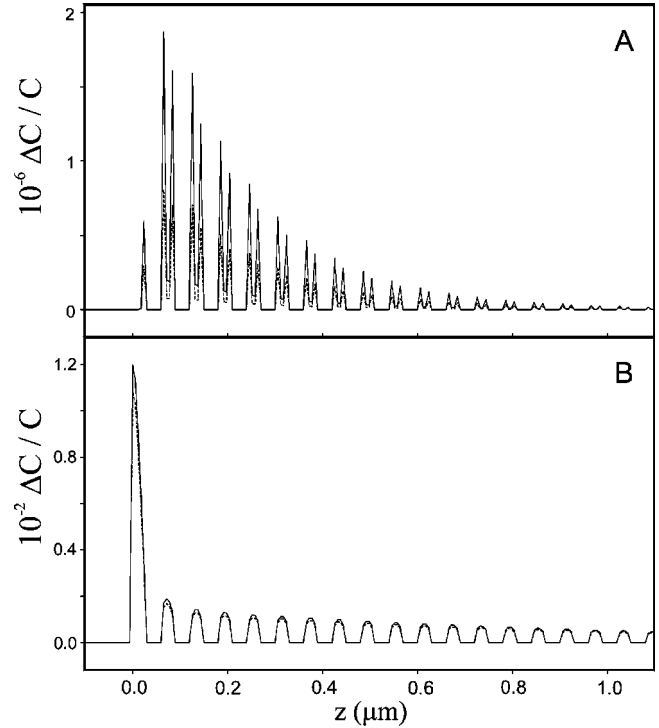


FIG. 4. Fractional collagen denaturation at the onset of vaporization at (A) 3 or (B) $6.45 \mu\text{m}$. Denaturation due to the FEL superpulse structure (solid) is compared to that due to a 16.2-ns pulse with the same average power (dashed). In (A), heat diffusion through both surfaces of each protein layer is evident.

This analytical approach allows us to investigate the influence of the superpulse structure, viewed as a train of picosecond pulses with a repetition rate of 2.85 GHz. In particular, a 16.2-ns pulse with the same average power as the superpulse exhibits similar thermal responses. However, as shown in Fig. 2 the longer pulse duration replaces the staircase and sawtooth with temperature ramps. Figure 4 indicates that the staircase associated with FEL irradiation leads to marginally greater accumulation of denatured collagen, i.e., picosecond pulses are not essential for this application. Instead, the key feature is the separation in layer temperatures as shown in Fig. 2, driven by the competition between the layer-specific heating rates and thermal diffusion.

IV. CONCLUDING REMARKS

We have tracked thermal diffusion in a laminar system, representative of cornea, as heated by a FEL at rates that satisfy the criterion for superheating of saline. At these temperatures and pulse durations, the model predicts no direct photothermal breaking of chemical bonds. However, at $6.45 \mu\text{m}$ the outer protein layers heat to temperatures sufficient to denature collagen on the 10-ns time scale. Consequently, $6.45\text{-}\mu\text{m}$ irradiation avoids the accumulation and subsequent propagation of stress energy seen at $3 \mu\text{m}$.

Although we modeled a very specific pulse structure and tissue geometry, these results can be generalized in two ways. First, the key dynamic processes occur within tens of nanoseconds, a consequence of the heterogeneous optical

and thermal properties of biomaterials. Thus, the preferential ablative properties of the FEL are a consequence of high average power on the 10-ns time scale as opposed to the specific superpulse structure. Second, while the laminar geometry of stroma renders the mathematics tractable, it is not essential to support the conclusions of this theoretical model. Diffusion is strongly geometry dependent and the tendency is for the diffusion rate to increase in cylindrical and especially spherical geometries. An increased diffusion rate would reduce the separation in layer temperatures and its subsequent effects. In contrast, the separation in layer temperatures would become more pronounced for larger protein assem-

blies, e.g., extracellular matrix. Subject to these competing influences, we expect similar effects to be observed whenever the rate of heat diffusion between the heterogeneous components of a biomaterial is slow compared to the rate of laser heating.

ACKNOWLEDGMENTS

This research has been supported by the DoD MFEL program as administered by the ONR through Grant No. N00014-99-1-0891 and the AFOSR through Grant No. F49620-00-1-0370.

-
- [1] G. Edwards *et al.*, *Nature (London)* **371**, 416 (1994).
 [2] M. Copeland *et al.*, *International Biomedical Symposium* (SPIE, San Jose, CA, 2000).
 [3] K. Joos *et al.*, *Lasers Surg. Med.* **27**, 191 (2000).
 [4] H. Davson, *The Physiology of the Eye* (Academic Press, New York, 1972).
 [5] J. Kampmeier, B. Radt, R. Birngruber, and R. Brinkmann, *Cornea* **19**, 355 (2000).
 [6] P. L. Privalov and E. I. Tiktopulo, *Biopolymers* **9**, 127 (1970).
 [7] J. J. Lim and M. H. Shamos, *Biopolymers* **13**, 1791 (1974).
 [8] L. Stryer, *Biochemistry*, 4th ed. (Freeman, New York, 1995), p. 32.
 [9] J. F. Liebman, H. Y. Afeefy, and S. W. Slayden, *The Amide Linkage* (Wiley, New York, 2000), Chap. V.
 [10] E. Spörl, U. Genth, D. Schmalfuss, and T. Seiler, *Ger. J. Ophthalmol.* **5**, 322 (1997).
 [11] J. M. J. Madey, *J. Appl. Phys.* **42**, 1906 (1971).
 [12] J. Tribble, D. C. Lamb, L. Reinisch, and G. Edwards, *Phys. Rev. E* **55**, 7385 (1997).
 [13] M. J. C. van Gemert and A. J. Welch, *Optical-Thermal Response of Laser-Irradiated Tissue* (Plenum Press, New York, 1995), Chap. XIII.
 [14] L. D. Landau and E. M. Lifshitz, *Fluid Mechanics*, 2nd ed. (Pergamon Press, Oxford, 1987), Chap. V.
 [15] A. W. Crook, *J. Opt. Soc. Am.* **38**, 954 (1948).
 [16] O. W. Shih, *J. Appl. Phys.* **75**, 4382 (1994).
 [17] K. D. Cole and W. A. McGahan, *J. Heat Transfer* **115**, 767 (1993).
 [18] L. G. Hector Jr., W.-S. Kim, and M. N. Özisik, *Int. J. Eng. Sci.* **30**, 1731 (1992).
 [19] V. P. Skripov *et al.*, *Thermophysical Properties of Liquids in the Metastable (Superheated) State* (Gordon and Breach Science Publishers, New York, 1988).
 [20] V. Venugopalan, N. S. Nishioka, and B. B. Mikić, *Biophys. J.* **70**, 2981 (1996).
 [21] D. Frank-Kamenetskii, *Diffusion and Heat Transfer in Chemical Kinetics*, 2nd ed. (Plenum Press, New York, 1969), Chaps. VI and VII.